# 1

# Force-Promoted Transformations in Mechanically Linked Molecules

*James Ormson[1], Anne-Sophie Duwez[2], and Guillaume De Bo[1]*

*[1] University of Manchester, Department of Chemistry, Oxford Road, Manchester M13 9PL, UK*
*[2] University of Liège, Molecular Systems, Department of Chemistry, Campus of Sart Tilman, Allee du Six aout, Liège 4000, Belgium*



## 1.1 Introduction

Mechanical bonds present useful dynamic properties that have been instrumental in the development of molecular machines and smart materials, as their subcomponents can undergo large internal displacement (e.g. shuttling of a macrocycle along the axle of a rotaxane) [1]. When coupled with a directional elongation force, such a large amplitude movement can trigger a useful mechanochemical transformation [2]. As an external force is applied, molecules respond by bond rotation and bending before cleavage of covalent bonds occurs at high force. Mechanical bonds follow a similar two-stage response to external force. If the macrocycle of a mechanical bond is forced away from its equilibrium position, the molecule will go through a stage of deformation (Figure 1.1, dashed arrows) before the eventual cleavage of a covalent bond (Figure 1.1, plain arrows). An alternative non-covalent dissociation pathway is accessible if the macrocycle can pass over the stopper of a rotaxane (dethreading).

Different experimental techniques can be used to study the two force ranges involved in the application of force to mechanically interlocked molecules. Single-molecule force spectroscopy (SMFS) has been used to probe non-covalent (e.g. elongation, dethreading) and dynamic (e.g. shuttling) processes in interlocked molecules. These phenomena typically occur in the pN regime, and SMFS provides quantitative information on the force and elongation distance involved. Ultrasound activation generates forces in the nN regime where the scission of covalent bonds occurs. This technique has been used to activate mechanically interlocked molecules and elucidate their mechanism of dissociation under tension. This chapter will cover the recent advances in the study of mechanical bonds under external force moving from low force (SMFS, Section 1.2) to high force (ultrasonication in solution, Section 1.3) processes. The final section presents the recent developments in the use of interlocked molecules in mechanoresponsive materials (Section 1.4).

*Mechanically Interlocked Materials: Polymers, Nanomaterials, MOFs, and more*, First Edition.
Edited by Emilio M. Pérez.

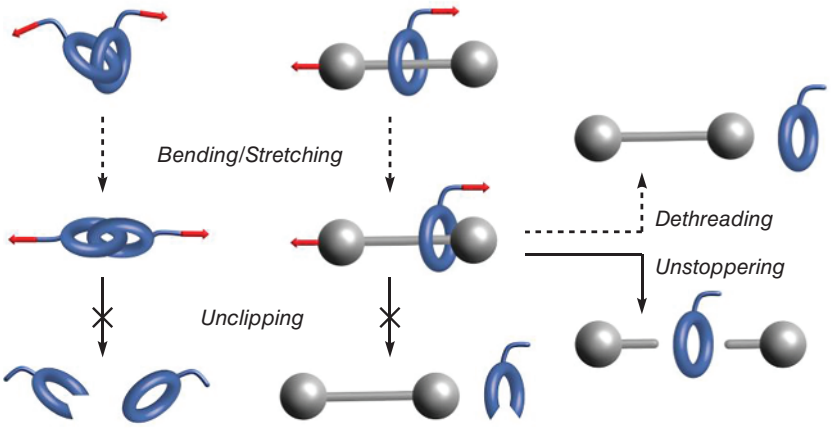


**Figure 1.1** Response of catenanes and rotaxanes to external force.

## 1.2 SMFS in the Study of Non-covalent Interactions

SMFS consists of trapping and stretching a molecule between an atomic force microscopy (AFM) tip and a surface, or in a laser trap or between magnetic beads, to probe molecular processes *in situ* and real-time through the application of mechanical forces. For more than two decades, SMFS has proved efficacious in deciphering mechanistic information of individual biomolecules and in quantifying their force response to external stress. Such experiments have provided unprecedented insights into the structure and function of many biological systems, including DNA, proteins, enzymes, and biomolecular machines [3–15]. In addition to its widespread use with biological macromolecules, the technique has been adapted for the study of intra-molecular processes in synthetic macromolecules, including polymers [16], mechanophores [17–20], and interlocked systems [21, 22]. However, only a few investigations on intra-molecular processes and single-molecule mechanics have been realized on small molecules (1–5 nm), with successful examples including molecular recognition pairing [23], helical structures [24], and artificial molecular machines prototypes [25–30]. The rarity of such studies stems from the difficulty in developing proper tools and preparing appropriate molecules that can be interfaced with SMFS techniques, especially when one wants to probe sub-molecular motions.

### 1.2.1 Rotaxanes

Stoddart, Houk, Ho, and coworkers have pulled the macrocycle over the bulky end groups of a redox-active rotaxane with an AFM tip [31]. They compared the large forces required to de-thread oxidized and unoxidized molecules. They have used the switchable, bistable, [2]rotaxane $\mathbf{R}^{4+}$ shown in Figure 1.2, whose mechanism is based on the redox-controlled mechanical shuttling of the macrocycle along its axis. The molecule was specifically designed with a short thioctic acid linker tethered to the ring for tight attachment to a gold AFM tip and with a hydroxymethyl group

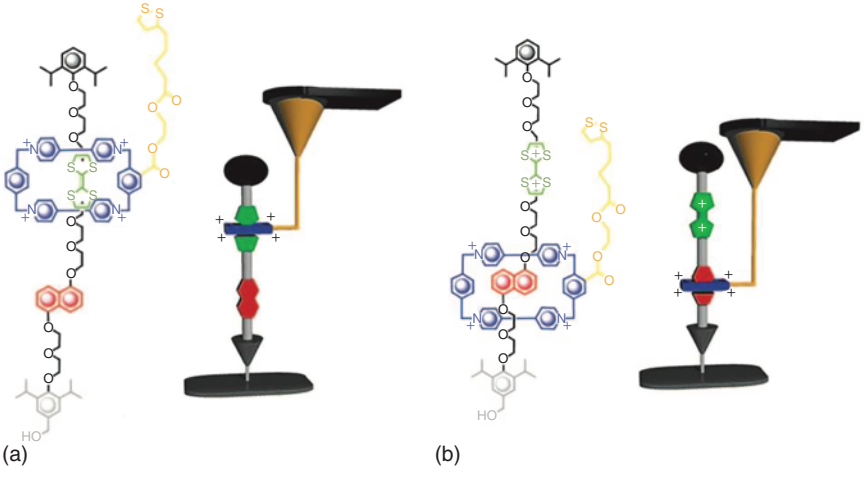


**Figure 1.2** Chemical structure and schematic representation of the AFM force spectroscopy experiment of the bistable [2]rotaxane $\mathbf{R}^{4+}$, in which an electron-poor cyclobis(paraquat-*p*-phenylene) ($CBPQT^{4+}$) ring is confined to an axis containing two electron-rich recognition sites, tetrathiafulvalene (TTF) and 1,5-dioxynaphthalene (DNP), by the presence of bulky 2,6-diisopropylphenyl ether stoppers at each end. The stopper close to the DNP site carries a hydroxymethyl group for subsequent attachment to silicon wafers. (a) The $CBPQT^{4+}$ ring, which carries a very short tether terminated by a thioctic acid ester for attachment to a gold-coated AFM tip, displays a stronger interaction with TTF than with DNP and thus resides selectively on the former. (b) Chemical oxidation of TTF to $TTF^{2+}$ results in a strong charge–charge repulsion between the $CBPQT^{4+}$ ring and $TTF^{2+}$, a situation that causes the $CBPQT^{4+}$ ring to shuttle to DNP in the oxidized [2]rotaxane $\mathbf{R}^{6+}$. Source: Brough et al. [31] / National Academy of Science.

on one of the stoppers for attachment to $SiO_2$ substrates via covalently bound monolayers of isocyanatopropyl linkers. They used force spectroscopy to probe the steric and electrostatic interactions present in the ground and oxidized states of $\mathbf{R}^{4+}$ (Figure 1.2). Control measurements consisted of probing molecules to measure the repulsive steric interactions between the cyclobis(paraquat-*p*-phenylene) ($CBPQT^{4+}$) ring and the diisopropylphenyl ether stopper. The probing of the $\mathbf{R}^{6+}$ molecules in an oxidizing solution was used to measure the repulsive force between the $CBPQT^{4+}$ ring and an oxidized tetrathiafulvalene ($TTF^{2+}$), which is responsible for molecular actuation. On the basis of the differences in the force required to pass the ring over the stopper in the presence and absence of the $Fe(ClO_4)_3$ oxidizing agent, they estimated the repulsive electrostatic barrier, which is ultimately responsible for the molecule's actuation.

By using the measured force spectroscopy values of 66 pN for the dethreading barrier under nonoxidative conditions and 145 pN for the oxidant-induced electrostatic repulsion barrier, along with the distance of 8.6 Å of the energy barrier produced from molecular simulations for the dethreading of the $CBPQT^{4+}$ ring over the bulky stopper, and 13.0 Å as the distance necessary for the $CBPQT^{4+}$ ring to travel from the 1,5-dioxynaphthalene (DNP) recognition site to the $TTF^{2+}$ dication, the difference in interaction energies can be calculated as 19 kcal $mol^{-1}$. By combining

the 19 kcal mol$^{-1}$ difference in oxidative and nonoxidative interaction energies with the theoretically determined value of 46 kcal mol$^{-1}$ for the energy associated with ground-state dethreading, a final value of 65 kcal mol$^{-1}$ was obtained, representing the amount of repulsive actuation energy between CBPQT$^{4+}$ and TTF$^{2+}$ produced by the oxidation of $\mathbf{R}^{4+}$. As estimated by this approach, 65 kcal mol$^{-1}$ represents the upper limit of the total actuation energy.

Unfortunately, the irreversible rupture of molecules due to the dethreading required by this experiment prohibits the realization of a relaxing step to complete the cycle required to directly probe the mechanical work generated against the external load and to verify the estimation of 65 kcal mol$^{-1}$.

In 2011, Duwez, Leigh, and coworkers succeeded in detecting sub-molecular movements in a hydrogen-bonded rotaxane and in directly measuring the work generated by this molecule against a load [25]. They designed a hydrogen-bonded rotaxane with a poly(ethylene oxide) (PEO) tether attached to the ring to track its motion by an AFM cantilever (Figure 1.3). The [2]rotaxane consists of a ring mechanically locked onto a thread by two bulky groups situated at either end of the axle. The thread bears a fumaramide and a succinic amide-ester site, each of which can bind to the macrocycle through four intercomponent hydrogen bonds [32]. The ring predominantly resides over the fumaramide site (green in Figure 1.3), the occupancy ratio being higher than 95 : 5, compared to the succinimide ester (orange in Figure 1.3). A chain, suitable for binding to an AFM tip, was attached to the macrocycle. Close to the fumaramide binding site, a 1,2-dithiolane ring was introduced to enable the grafting of the rotaxane onto a gold surface.

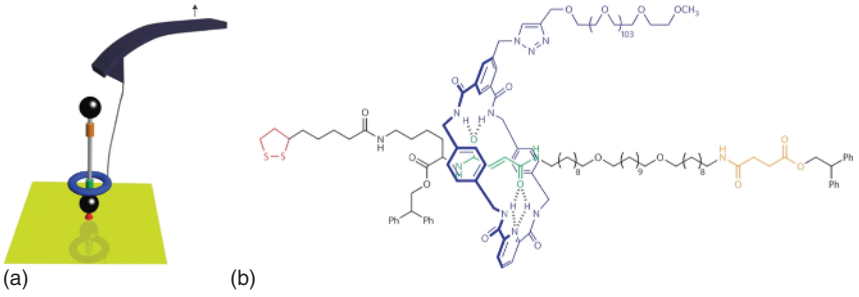


**Figure 1.3** (a) Schematics of the single-molecule force spectroscopy experiment of the rotaxane. The rotaxane is grafted onto gold, and the PEO tether is caught by the AFM tip. (b) Chemical structure of the rotaxane molecule. The rotaxane consists of a benzylic amide molecular ring (in blue) mechanically locked onto an axle by bulky diphenylethyl ester groups situated at either end. The axle bears a fumaramide group (in green) and a succinic amide-ester group (in orange), either of which can act as a binding site for the ring through up to four intercomponent hydrogen bonds. The affinity of the ring for the fumaramide site is much higher than for the succinic amide-ester site so the fumaramide: succinic amide-ester occupancy ratio is higher than 95 : 5. Next to the fumaramide binding site, a disulfide group (in red) was introduced to enable the grafting of the molecule onto gold substrates. A PEO tether (in blue) is attached to the ring in order to link the molecule to the AFM probe and track the motion of the ring along the axle. Source: Lussis et al. [25] / Springer Nature.

They used the cantilever of an AFM microscope to catch the tether, then applied a mechanical load to the ring of the rotaxane and followed its movement. The caught molecules were stretched in a controlled manner by moving the tip away from the substrate at a fixed pulling rate, and the force–extension profiles were measured. Thanks to the long tether, the detachment of the macrocycle from its station is directly observable in the stretching profile. Indeed, the progressive stretching of the PEO tether gives the characteristic parabolic profile of a random coil, which loses entropy on stretching, inducing a restoring force. Once the force exerted on the tether exceeds the strength of the hydrogen bonds between the macrocycle and the fumaramide station, the hydrogen bonds break, which results in the appearance of a small peak in the main force profile. This peak appears at about 27 pN in dimethylformamide and 45 pN in tetrachloroethane (TCE), reflecting the relative strengths of solute–solute hydrogen bonding in the two solvents. They fitted the pulling profiles with the worm-like chain model (an entropic elasticity model that predicts the relationship between the extension of a linear polymer and the entropic restoring force). The fits of the profile before and after the rupture peak give the increase in length ($\Delta L_c$) of the molecule after the rupture of the inter-component hydrogen bonds of about 4 nm, which is consistent with the theoretical length of the fully extended thread between the two binding sites.

Pulling–relaxing cycles were also recorded, and they observed a peak, which is the signature of force acting on the tether. This shows that the macrocycle has traveled back from the succinic amide-ester site to the fumaramide site and that it is able to generate force when rebinding against the external load exerted by the cantilever. It means that if we trap the ring and then slightly decrease the force on the tether while maintaining the pulling, the ring is capable of pulling more strongly to recover its preferred position. In TCE, the macrocycle is able to travel back against an external load of 30 pN. The mechanical work produced by this sub-molecular motion is about 6 kcal mol$^{-1}$.

They also used the Crooks fluctuation theorem to estimate the free energy driving the macrocycle to bind to the fumaramide binding site at zero force. The work done on/by the molecules during pulling/relaxing is given by the areas below the corresponding force–extension curves. The rupture and rebinding work distributions overlap over a large range of work values and cross at a value of the work $\Delta G$ of $9.3 \pm 2.3\ k_B T = 5.5 \pm 1.3$ kcal mol$^{-1}$. The work value for a loading rate of 500 pN s$^{-1}$ is close to this binding-energy difference between the two hydrogen-bonding motifs, indicating that under these conditions, the rotaxane is able to make use of almost all the energy available from hydrogen bonding to perform work along the direction of the applied load.

This example was the first quantitative measurement of the work done by a single synthetic molecular machine. It shows that the biased Brownian motions caused by thermal energy can be harnessed within a single synthetic small molecule to generate significant directional forces of similar magnitude to those generated by natural molecular machines, which are a lot bigger.

More recently, they detected the real-time fluctuations in the force experiments on these rotaxanes and revealed an intermediate weak binding state during

shuttling [30]. They mechanically triggered the translocation of the ring between the two principal binding sites on the axle. Equilibrium fluctuations reveal another interacting site involving the two oxygen atoms in the middle of the thread. They characterized the ring occupancy distribution over time, which confirms the intermediate in both shuttling directions. The study provides evidence of weak hydrogen bonds that are difficult to detect using other methods and shows how the composition of the thread can significantly influence the shuttling dynamics by slowing down the ring motion between the principal binding sites. More generally, the study illustrates the utility that single-molecule experiments, such as force spectroscopy, can offer for elucidating the structure and dynamics of synthetic molecular machines.

Ibarra and coworkers studied the dynamics of a related rotaxane, modified to contain a very long thread so that the molecule could be investigated using optical tweezers in an aqueous environment (Figure 1.4) [27]. Force-clamp experiments under low external forces were made possible due to the high stability of the trapping, which allowed them to measure the dynamics of the rotaxane in an aqueous medium. They observed a lower rupture force of 8.5 pN for the breaking of hydrogen bonds between the macrocycle and the fumaramide station, in agreement with the relative strengths of hydrogen bonding in water and organic solvents, intercomponent hydrogen bonds being stronger in less polar solvents. Hopping events were also evidenced between the fumaramide and succinic amide-ester stations, but no intermediate states were observed. Since these experiments were performed in aqueous conditions, we suggest that the formation of weak hydrogen bonds between the macrocycle and the polyether thread would be much less favorable, and so, under those experimental conditions, the intermediate states may not be significant. Furthermore, the detection of such close intermediate states is difficult, given the spatial resolution of optical tweezers.

Their experimental set-up allowed very stable pulling–relaxing experiments to probe real-time shuttling events. Under these conditions, hundreds of shuttling events of the macrocycle between the two stations were monitored in real-time during minutes. From these data, they obtained crucial information about the dynamics of shuttling and a detailed picture of the energy landscape at different forces.

In 2018, Duwez, Sluysmans, Stoddart, and coworkers investigated the mechanochemical properties of donor–acceptor oligorotaxane foldamers, in which interactions between the mechanically interlocked component parts dictate the single-molecule assembly into a folded secondary structure (Figure 1.5) [28].

They used AFM-based SMFS to mechanically unfold molecules made of oligomeric dumbbells incorporating DNP units encircled by $CBPQT^{4+}$ rings. Real-time capture of fluctuations between unfolded and folded states revealed that the molecules exert forces of up to 50 pN against a mechanical load of up to 150 pN and displayed transition times of less than 10 μs. They showed that the folding is at least as fast as that observed in proteins and remarkably more robust, thanks to the mechanically interlocked structure.

The mechanical breaking of the donor–acceptor interactions responsible for the folded structure was measured over a broad range of loading rates [29]. The

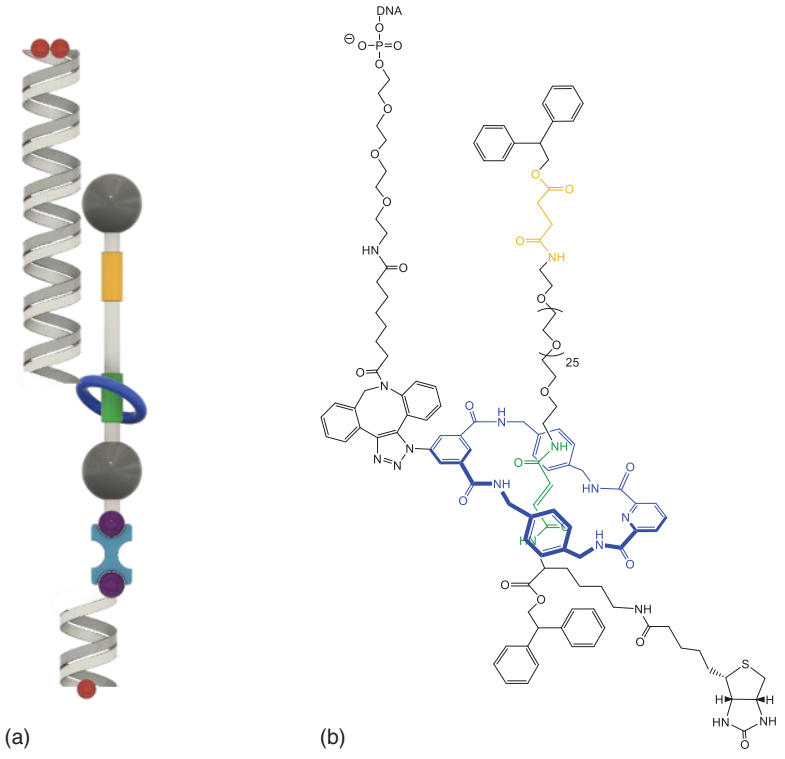


**Figure 1.4** (a) Schematics of the OT-based single-molecule force spectroscopy experiment of the rotaxane. The rotaxane is attached to two polystyrene beads (diameter ~3 μm) through two dsDNA molecules: the 2686 bp dsDNA molecule connects the macrocycle to the bead via digoxigenin–antidigoxigenin (Dig–αDig) connections. The 830 bp dsDNA molecule connects the shuttle to a bead held by suction on a micropipette, via biotin–streptavidin connections at one end and Dig–αDig at the other end. Load is applied to the system by moving the optical trap away from the micropipette. At constant load, the shuttling dynamics of the macrocycle are inferred by measuring the motions of the bead. (b) Chemical structure of the rotaxane molecule modified to be trapped in a laser in an aqueous medium. The axle contains fumaramide (green) and succinic amide-ester (orange) stations separated by a very long oligoethyleneglycol spacer. A DNA oligonucleotide was covalently attached to the macrocycle to allow the manipulation in the optical trap.

results showed a high constant rupture force over a leading rate covering three orders of magnitude. In comparison with dynamic force spectroscopy performed during the past 20 years on various (bio)molecules, the near-equilibrium regime of oligorotaxanes persists at much higher loading rates, at which biomolecules have reached their kinetic regime, illustrating the high-speed dynamics and remarkable rebinding capabilities of the intramolecular donor–acceptor interactions. The authors investigated single interactions at a time in pulling–relaxing cycles and evidenced the near-equilibrium stochastic behavior. Indeed, even if the pulling experiments are performed near thermodynamic equilibrium, small molecules are always being submitted to random thermal fluctuations that constantly modify their unfolding and refolding paths. Using the Crooks fluctuation theorem, they measured the mechanical work produced during the breaking and rebinding to

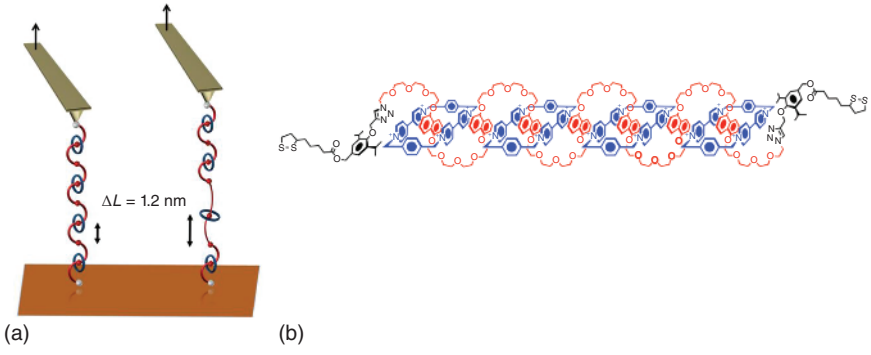


**Figure 1.5** (a) Schematics of the single-molecule force spectroscopy experiment of the oligorotaxane. The theoretical variation of length after breaking one interaction between a free DNP and the contiguous ring is about 1.2 nm, on the basis of crystallographic data. (b) Chemical structure of the oligorotaxane molecule made of oligomeric dumbbells incorporating 1,5-dioxynaphthalene units encircled by cyclobis(paraquat-*p*-phenylene) rings.

determine a free-energy difference, $\Delta G$, of 6 kcal mol$^{-1}$ between the two local conformations around a single bond.

### 1.2.2 Poly-(pseudo)rotaxanes

In contrast to rotaxanes, pseudorotaxanes are kinetically labile as their macrocycle is able to dethread spontaneously (i.e. the stoppers are too small to retain the macrocycle). This ability has been studied experimentally [33–40] and computationally [33, 35, 41], and subsequent mechanochemical studies have provided information of the forces needed to overcome steric groups and distinguish rotaxanes from pseudrotaxanes. Cyclodextrins (CD) spontaneously form pseudorotaxanes by threading onto polyethyleneglycol (PEG) chains [42], and the dethreading behaviour of these systems has been studied by Round and co-workers in 2008 [43]. Polyrotaxanes of varied lengths were probed by AFM (Figure 1.6). Pulling experiments at loading rate in the range of 7–12 nN s$^{-1}$ indicate a rupture force around 114 pN with a rupture length corresponding to length of the PEG axle and the length of the tip tether. This observation, and the fact that the detachment of the of the polymer from the tip occurs at a higher force, suggests that the rotaxane disassembles with the dethreading of CD macrocycle over the bulky tricarboxylic acid benzoyl stopper.

The same authors have used a CD-based pseudorotaxane to measure the strength of a calcium-mediated eggbox junction (a cross-link between sequences of oligoguluronic acids [oligoGs]) [44]. After some equilibration time, an AFM tip was used to pick an α-CD in order to unzip the eggbox junction. The authors determined how much force is required to slide along a single strand of oligoGs. Slipping over one guluronic acid requires about 47 pN, while unzipping requires 58, 112, and 141 pN (at 6–20 nN s$^{-1}$) for oligoGs containing 2, 4, and 8 $Ca^{2+}$, respectively. The strength of the first cross-link depends on the number of subsequent cross-links, and inspection of the force–extension curves of the different oligomers show that the CD does not break one complex at a time but rather disrupts a sequence of four $Ca^{2+}$ at once.

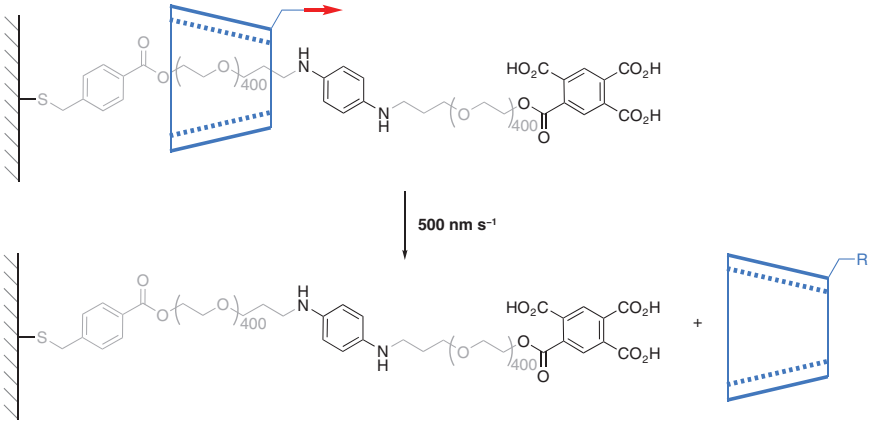


**Figure 1.6** Single-molecule force spectroscopy experiment of the deslipping behavior of α-CD over a tricarboxylic acid benzoyl stopper on a PEG track. The red arrow indicates the direction of force.

The same group used a similar design measure the strength of a calcium-mediated eggbox junction (a cross-link between sequences of oligoguluronic acids [oligoGs]) [44]. After some equilibration time, an AFM tip was used to pick an α-CD to unzip the eggbox junction. They found that this macrocycle requires ~47 pN to slip over one guluronic acid, while unzipping requires 58, 112, and 141 pN (at 6–20 nN $s^{-1}$) for oligoGs containing 2, 4, and 8 $Ca^{2+}$, respectively. Inspection of the force-extension curves showed that the first cross-link is influenced by the subsequent cross links causing 4 $Ca^{2+}$ units to break in a single event.

They also exploited the sliding and deslipping behavior of α-CD to map the position of specific groups along a polymer chain and called their approach "sliding contact force spectroscopy" [45].

### 1.2.3 Catenanes

In 2014, Duwez, Fustin, Leigh, and coworkers probed the mobility of the rings in a [2]catenane of the benzylic amide family [26]. They selected two catenanes that differ only by methylation of the amide groups and the corresponding ability to form inter-component hydrogen bonds (Figure 1.7). Catenane CatNH has secondary amide groups and can thus form hydrogen bonds between the two macrocycles, restricting their mobility. In catenane CatNMe, the amide groups are methylated, and the rings are relatively free to rotate. PEO chains were grafted at each side of the catenane for pulling with the AFM tip. The experiment consisted of performing approach-retraction cycles with the AFM tip on the molecules adsorbed on the substrate in both TCE and DMF. The persistence length of each molecule was extracted by fitting the force–extension curves with a worm-like chain model.

Catenane CatNMe, which is unable to form any internal hydrogen bonds, showed the same persistence length ($L_p$) in both solvents (0.45 nm). In contrast, catenane CatNH showed a large increase in $L_p$ from DMF (0.5 nm) to TCE (1 nm), due to strong hydrogen bond interactions between the two macrocycles that transform the

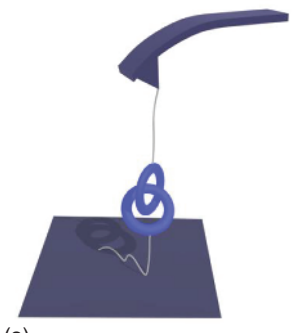

(a)

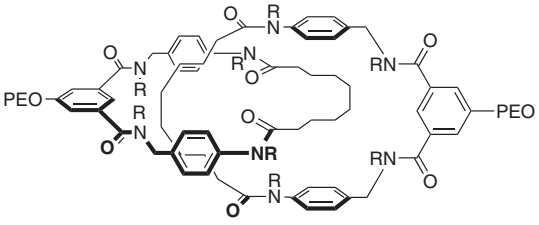


(b)

**Figure 1.7** (a) Schematics of the single-molecule force spectroscopy experiment of the catenane. (b) Chemical structure of the [2]catenane of the benzylic amide family.

catenane in a long rigid segment. This result showed that SMFS is able to address the mobility of the rings of a single catenane unit, and demonstrates the impact that a single mechanical bond can have on the mechanical properties of polymers.

In 2019, Zhang, Huang, and coworkers investigated a poly[2]catenane made of the same catenane units of the benzylic amide family with inter-component hydrogen bonds (Figure 1.8) [22]. The catenane units are separated by short alkane tethers. When pulling on these polymers, they observed force–extension curves with a regular sawtooth pattern containing evenly spaced peaks. The contour

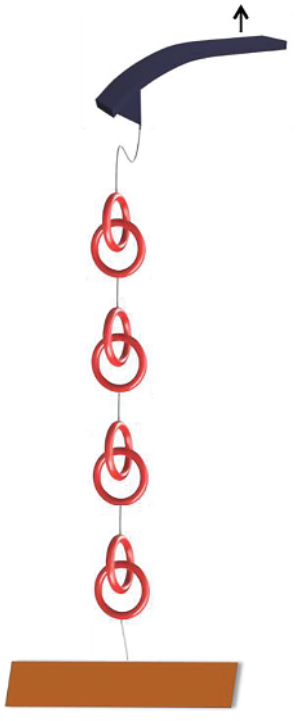

**Figure 1.8** Schematics of the AFM-based single-molecule force spectroscopy experiment of a poly[2]catenane.

length increments, $1.68 \pm 0.12$ nm, were in good agreement with the length change expected (1.5 nm) after the rupture of the inter-component hydrogen bonds from the theoretical modeling of the structures. They performed the pulling experiments at eight different pulling rates and determined the characteristic force rupture for the inter-component hydrogen bonds. They could observe both the equilibrium (below ~1500 pN $s^{-1}$) and kinetic regimes (above ~1500 pN $s^{-1}$). Kinetic and thermodynamic parameters of the dissociation were extracted from the data with the Bell–Evans model [46]. The spontaneous unbinding rate in the absence of external force was estimated at about 0.07 $s^{-1}$, and the distance between the bound state and the transition state was estimated at about 2.82 Å. Since the near-equilibrium regime is probed, it would be interesting to re-analyze the data with the Friddle–Noy–De Yoreo model that consists of a nonlinear fit including both the near-equilibrium (loading rate-independent) and the kinetic regimes where the force is proportional to the logarithm of the loading rate [47]. Cycles of one pulling and one relaxing experiment were also realized and showed that the hydrogen bonds can reform between the macrocycles of the catenanes during the relaxing step. The rebinding force was determined at the different loading rates. The spontaneous rebinding rate was estimated at $3.6 \times 10^5$ $s^{-1}$, and the distance between the unbinding state and the transition state was estimated at 3.51 Å, using the Bell–Evans model.

Janshoff, Marszalek, and coworkers designed an oligomer system made of interlocked calix[4]arenes dimers [21]. The dimers are held together by 16 hydrogen bridges, and the interlocking limits how far the dimers can be separated after the rupture of the H bonds (Figure 1.9). The design prevents the bond rupture from being irreversible and thus enables the study of the rebinding of the calix[4]arenes dimers. Oligomers were prepared by tethering several of these dimers together. The force–extension curves obtained by pulling the molecule displayed a regular sawtooth pattern indicative of the successive rupture of the calixarene dimers.

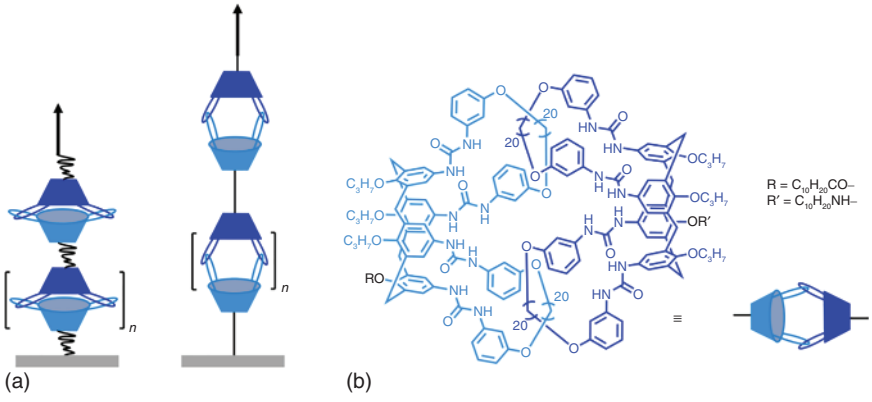


**Figure 1.9** (a) Schematics of the AFM-based single-molecule force spectroscopy experiment of interlocked calix[4]arenes dimeric capsules. (b) Chemical structure of the capsules bound together by 16 hydrogen bonds.

The assignment of the peaks was unambiguous in light of their equidistance, which corresponds to the theoretical distance for the dimer separation. The strength and reversibility of the hydrogen bonds were measured at various loading rates, covering both the equilibrium regime and out-of-equilibrium regime, corresponding to pulling rates close to the spontaneous bond dissociation rate or much higher than this rate, respectively. The results, together with stochastic modeling using a three-well potential under external load, allowed the reconstruction of the energy landscape of the system.

## 1.3 Strength of Mechanical Bonds

In polymer mechanochemistry, polymer chains are used to activate mechanophores (force-sensitive molecules) in a way reminiscent of a tug of war. This can be achieved in solution with ultrasound-induced cavitation, where acoustic waves cause the nucleation, growth, and collapse of microbubbles. As bubbles collapse, a high gradient elongational flow is created in the surroundings, causing a nearby macromolecule to be stretched until covalent bond scission occurs in the central region of the chain [48]. This technique has been used to activate a variety of mechanophores [49], sometimes along unusual reaction pathways [50–52], prepare functional materials [53], carry out *in situ* catalysis [54, 55], or induce the release of small molecules [56], among others. Similarly, a mechanical bond at the center of a polymer chain will be subjected to a much higher strain rate than what can be achieved by SMFS, allowing for the dissociation pathways to be explored. These studies have revealed that dissociation via unclipping is unlikely since macrocycles can spread tensional stress around their circumference (Figure 1.1). As a result, rotaxanes break preferentially by unstoppering, as bonds in the axle are weakened, while catenanes act as a mechanochemical protecting group, as tensional stress accumulates in the linear segments outside the catenane (see below).

### 1.3.1 Polymers Containing a Rotaxane

The first investigation into the strength of the mechanical bond was carried out by Stoddart and coworkers in 2011, with the activation of polymers containing rotaxane mechanophores at the center by sonication [57]. In this technique, macromolecules are elongated by solvodynamic shear in the vicinity of collapsing ultrasound-induced cavitation bubbles [58]. The activation of polymers containing $CBPQT^{4+}$-derived [2]-rotaxanes (Figure 1.10) was compared to the linear and rotaxane end group polymers as controls. Diminution of the charge-transfer UV–vis absorption, associated with the interaction between the ring and the electron-rich DNP unit, was higher for the rotaxane-centered polymer compared to the controls as the applied force pulls the macrocycle away from the DNP unit. Although the authors provided no further details of the possible dissociation mechanism of the rotaxane, an earlier AFM study by the same group showed how a similar rotaxane was disassembled

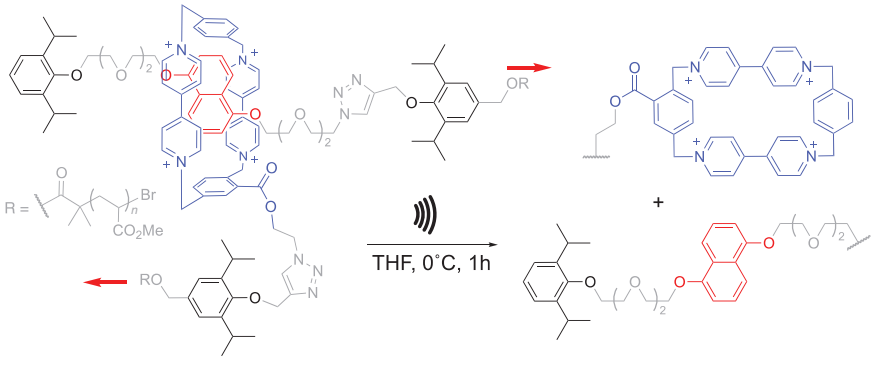


**Figure 1.10** Mechanical activation of Stoddart's rotaxane in the center of a poly(methyl acrylate) backbone, red arrows indicate the direction of force, counter ions not shown for clarity.

by dethreading of a $CBPQT^{4+}$ macrocycle over the same diisopropylphenyl stopper at a force much lower than that needed for the cleavage of a covalent bond [31]. This is further supported by recently constrained geometries simulate external force (CoGEF) calculations, which predict the dethreading of the macrocycle at a force of 0.96 nN [59].

To shed light on how entanglement can affect the mechanical reactivity of a covalent bond, Zhang and De Bo studied the activation of a Diels–Alder (DA) mechanophore placed in the axle of a rotaxane [60], where a benzo-21-crown-7 (B21C7) macrocycle is stoppered on one side by a mechanically active *proximal-exo* DA adduct (i.e. an DA adduct of *exo* configuration where the polymer handle is close to the furan/maleimide junction) [61] and on the other side by a large stopper that prevents any dethreading even under tension (**1**, Figure 1.11). Upon elongation of the rotaxane, the macrocycle is pulled away from the ammonium binding station until it reaches the large stopper. As it is unable to cross the steric obstacle, tension increases in the macromolecule until the dissociation of the DA mechanophore.

The mechanical activation was performed using high-intensity ultrasound (20 kHz, 11.5 W $cm^{-2}$, 1 s ON/2 s OFF). The dissociation of the mechanophore and the generation of rotaxane **2** (the resulting maleimide is a stopper for B21C7) was confirmed by $^1$H NMR. The mechanical activation of rotaxane **1** was slower than its force-uncoupled rotaxane **3** (in which the macrocycle is not covalently linked to the polymer backbone and hence not coupled to the force) and axle **4** counterparts. In other words, the mechanical activation of a DA mechanophore is slower when a rotaxane is used as a force actuator. The difference in reactivity originates from the constriction of the axle by the stretched macrocycle, which induces a significant amount of deformation in the chain and results in the accumulation of tensile, bending, and torsional stress in this region of the rotaxane. The presence of a competing high-stress region effectively decreases the mechanical coupling (i.e. how much the bond elongates as the mechanophore is stretched) of the scissile bond in the mechanophore, which in turn reduces the rate of activation. This region is unique to the rotaxane architecture, and the replacement of the *proximal-exo*

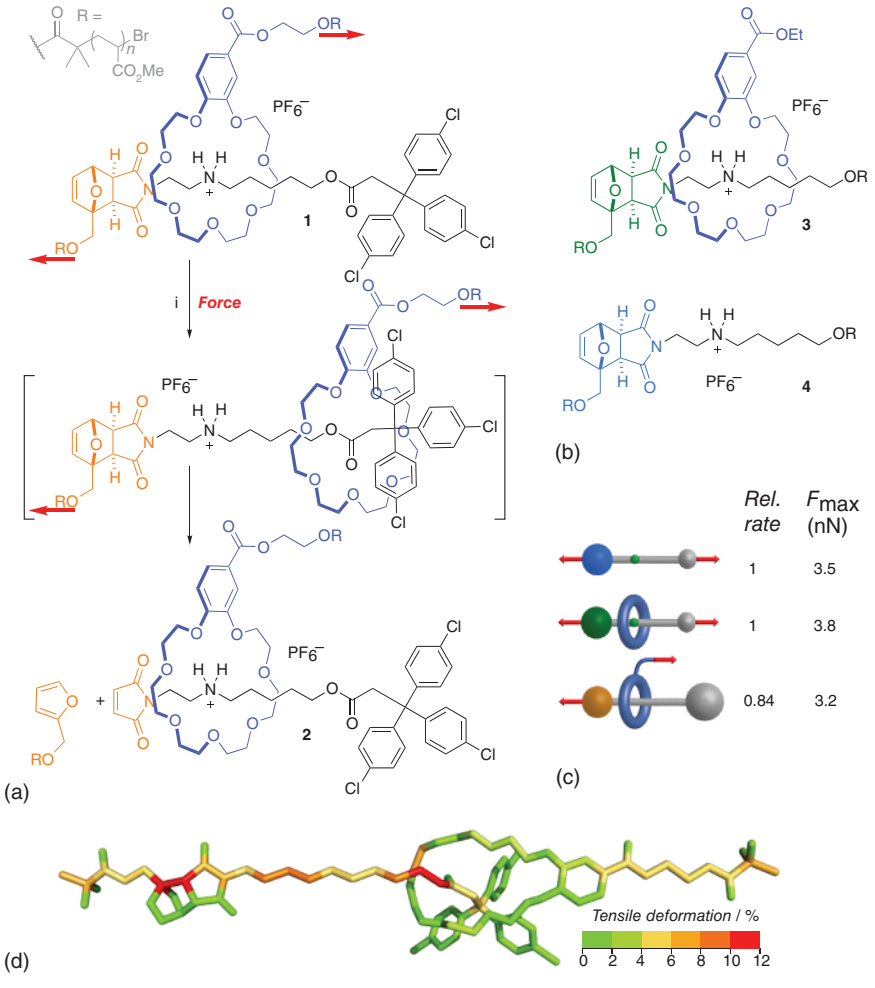


**Figure 1.11** Rotaxane as a force actuator in a Diels–Alder reaction. (a) Mechanical activation of rotaxane **1**. (i) US (20 kHz, 13.0 W cm$^{-2}$, 1 s ON/2 s OFF) THF, 5–10 °C, 240 min. Red arrows indicate the direction of force. (b) Uncoupled rotaxane and linear mechanophore were used as controls. (c) Relative rates of dissociation and maximum force before cleavage of mechanophores. (d) Distribution of tensile stress in rotaxane mechanophore obtained from CoGEF calculations (DFT B3LYP/6-31G*).

DA mechanophore by a mechanically inert *distal-exo* DA adduct suggests the possibility of a selective cleavage of the terminal bulky stopper [62]. In this case, CoGEF calculations show the presence of a unique high-stress region centered on the axle-stopper junction (Figure 1.12b). Sonication of rotaxane **5** confirmed the predicted unstoppering dissociation pathway, as carboxylic acid **6** was isolated from the post-sonication mixture along with macrocycle- and amine-terminated polymers **7** and **8** respectively (as the linker joining the stopper to the ammonium station is eliminated in the process). These results suggest that the rotaxane cleaves via an unstoppering pathway, which is initiated by the homolytic scission of the

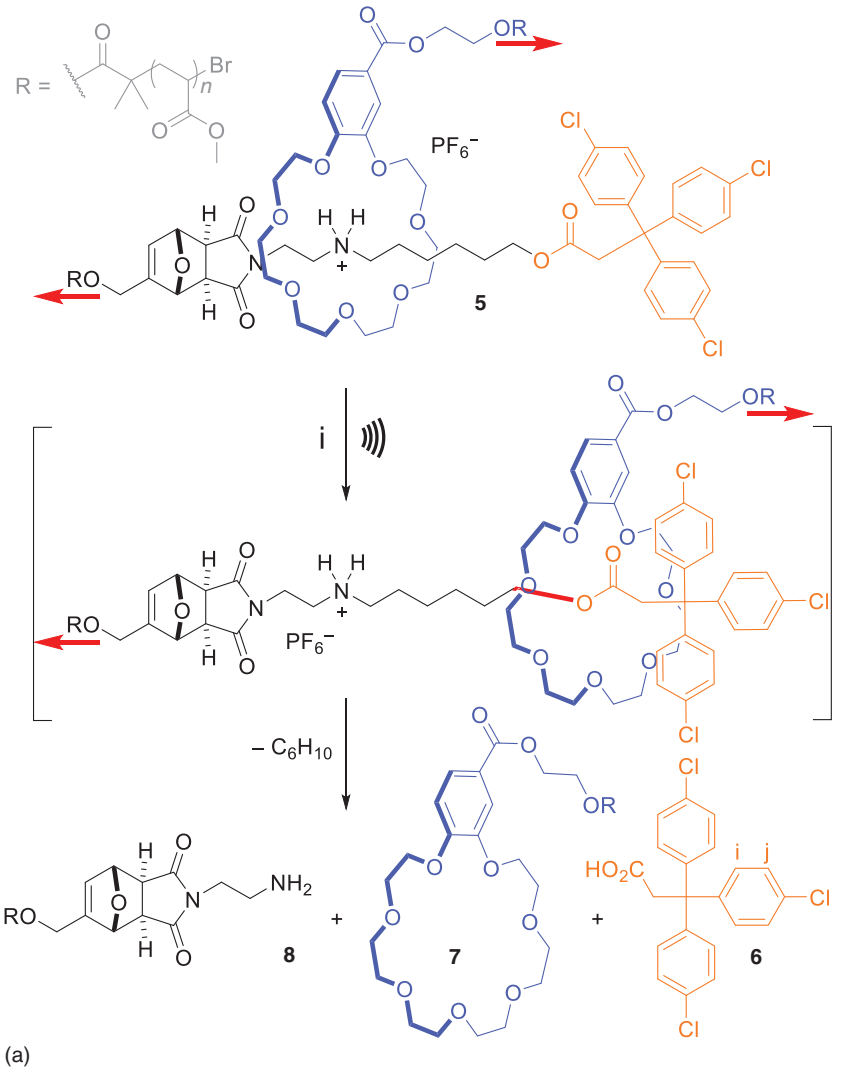


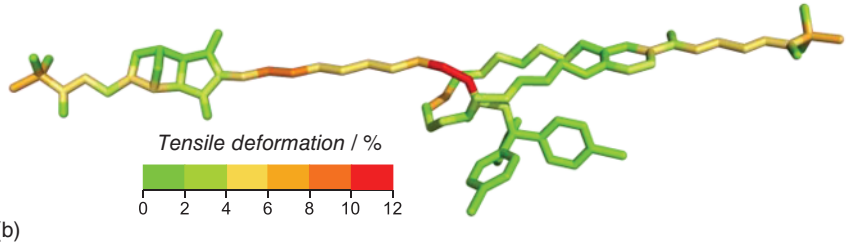


**Figure 1.12** (a)Mechanical dissociation of rotaxane mechanophore **5** by an unstoppering process. (i) US (20 kHz, 11.5 W $cm^{-2}$, 1 s ON/2 s OFF), $CH_3CN$, 5–10 °C, 240 min. Red arrows indicate the direction of force. (b) Distribution of tensile stress in rotaxane mechanophore obtained from CoGEF calculations (DFT B3LYP/6-31G*).

C—O bond at the axle-stopper junction. This bond is only observed to cleave in rotaxane **5**, as its force-uncoupled rotaxane and axle counterparts cleave in the poly(methyl acrylate) backbone. This selectivity originates from the constriction of the axle by the stretched macrocycle, resulting in the accumulation of high tensile, bending, and torsional stress that active covalent bonds that are otherwise unreactive. In other words, a rotaxane actuator enhances the mechanical reactivity of the covalent bond in the axle. This finding has significant implications for the future development of slide-ring materials (a network of polyrotaxanes connected by their macrocycles) [63]. They display a remarkable ability to absorb mechanical energy at low extension due to "pulley effect" of their mobile cross-links, but this finding suggests that their rotaxane architecture could accelerate the failure of this material at maximal elongation (when the macrocyclic crosslinks are forced against the terminal stoppers of the polymer axles).

### 1.3.2 Polymers Containing a Catenane

As rotaxane actuators are able to induce a substantial amount of deformation in the axle (Figure 1.12b), it is noteworthy that the macrocycle itself is virtually free from

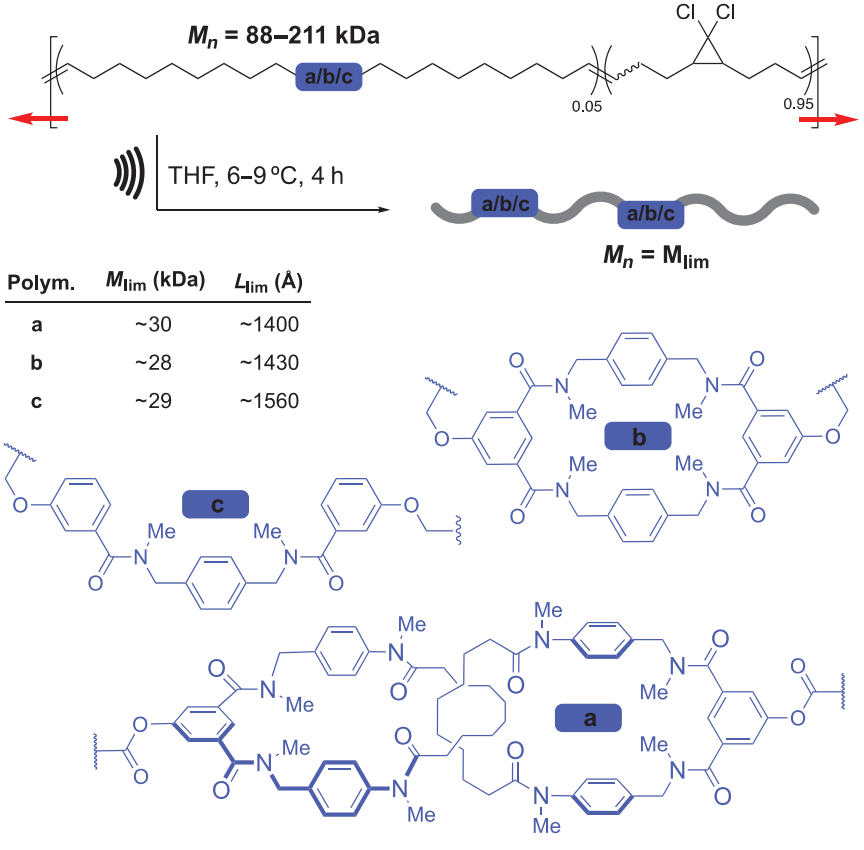


| Polym. | $M_{lim}$ (kDa) | $L_{lim}$ (Å) |
|---|---|---|
| a | ~30 | ~1400 |
| b | ~28 | ~1430 |
| c | ~29 | ~1560 |

**Figure 1.13** Sonication data for Craig' s polymers. Limiting mass and length of polymers containing a catenane (a), compared to macrocyclic (b), and linear (c) controls. Red arrows indicate the direction of force.

deformation. Indeed, because tension can spread over the entire circular backbone of macrocycles, they are less susceptible to elongational deformation than linear segments.

In an early study, Craig and coworkers have shown that copolymers containing [2]catenane junctions were as strong as their non-interlocked and linear counterparts. Multi-mechanophore gem-dichlorocyclopropanatedpolybutadiene copolymers with 5 mol% of either a benzamide [2]catenanes, or a macrocyclic or linear mimic were sonicated for a prolonged time in order to reach the limiting molecular weights ($M_{lim}$) below which mechanical activation does not occur [64]. All three polymers show similar limiting molecular weights ($M_{lim}$) and limiting lengths ($L_{lim}$), which confirms their similar mechanochemical reactivity (Figure 1.13).

The previous results suggest that bond scission occurs outside the topological features of these polymers (i.e. in the linear segments in between); however, the location and nature of the scissile bond were not investigated. This issue was tackled in a

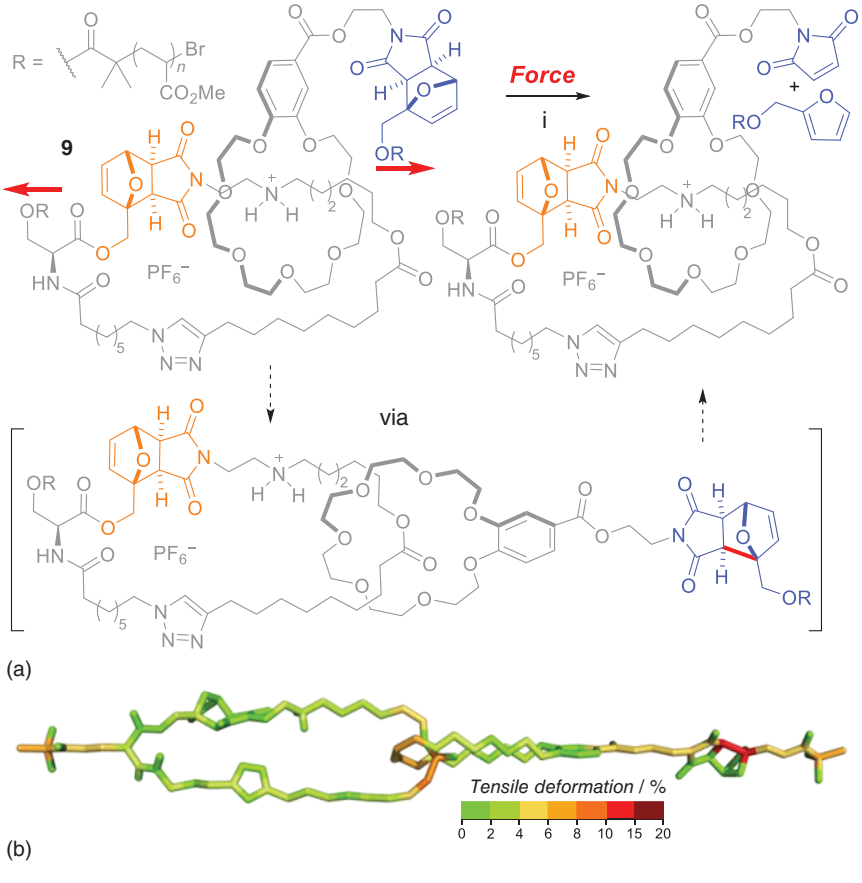


**Figure 1.14** Mechanical activation of catenane mechanophore **9**. (i) US (20 kHz, 13.0 W cm$^{-2}$, 1 s ON/2 s OFF), $CH_3CN$, 5–10 °C, 240 min. Red arrows indicate the direction of force. (b) Distribution of tensile stress in catenane mechanophore obtained from CoGEF calculations (DFT B3LYP/6-31G*).

recent study by Zhang and De Bo, where they investigated the mechanical activation of a [2]catenane containing two identical mechanophores, one placed inside the main ring of the catenane and the other one in the linear segment joining the other ring to the actuating polymer (Figure 1.14a) [65]. The catenane is formed of a B21C7 macrocycle threaded onto a larger 39-membered ring macrocycle and contains two identical *proximal-exo* DA mechanophores. The *intracyclic* mechanophore is embedded in the main ring, while the *extracyclic* mechanophore separates the smaller B21C7 macrocycle from the actuating polymer. Sonication of catenane **9** leads to the sole activation of the *extracyclic* mechanophore. Indeed, as the catenane is stretched, the macrocycles will rotate along each other to a position where the tension is spread equally over the two rings. As a result, the *intracyclic* mechanophore experiences a much lower level of deformation than its *extracyclic* counterpart in the linear section of the construct (Figure 1.14b).

## 1.4 Changes in Optical Properties – Reversible and Irreversible Changes of Optical Properties by Movement of Macrocycle in a Rotaxane

External force can also be applied to polymers containing mechanical bonds in the solid state. This activation has previously been used in the development of irreversible force sensors as the cleavage of covalent bonds in mechanophores gives an optical response [66]. Polymers containing mechanical bonds provide access to reversible force probes. Gradually applying force in the solid state will first disrupt weak non-covalent interactions in the mechanophores, followed by bond dissociations as the force is increased or many cycles are applied. This behavior has resulted in the development of optical force sensors that act both reversibly and irreversibly and have the ability to visualize both small and large forces.

Slide ring gels contain polymer chains that are covalently cross-linked by a figure of eight cross-links. These cross-links are neither covalently linked to nor have physical interactions with the polymer chains, allowing for the links to pass over the chains, causing the dispersion of applied tension over the material. The slide ring effect causes these gels to have improved mechanical properties compared to polymers containing covalent cross-links [63].

In an effort to visualize the slide-ring effect, Takata, Otsuka, and coworkers assembled a slide-ring gel in which macrocycles are connected by a diarylbibenzofuranone (DABBF) [67] mechanochromophore [68]. As the gel is stretched, mechanical energy is dissipated via the sliding of the macrocycle (slide-ring transition). In this context, the DB24C8 macrocycle is pulled away from the secondary ammonium station over the C12 linker until it reaches the terminal 2,5-dimethylphenyl stopper. Further elongation would activate the DABBF mechanochromophore to produce a blue-colored arylbenzofuranone (ABF) stable radical, effectively revealing where a slide-ring transition has occurred (Figure 1.15a). Covalent (CCP) and rotaxane (RCP) cross-linked polymers were formed by reacting a methyl acrylate (MA)-based random copolymer modified with 3-isopropenyl-α,α-dimethylbenzyl isocyanate

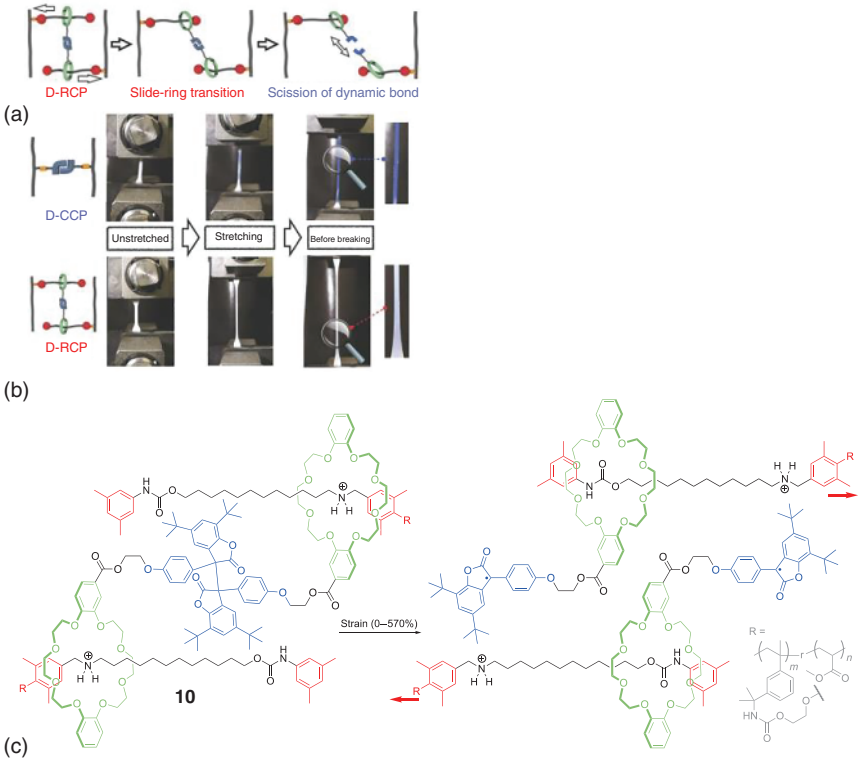


**Figure 1.15** (a) Schematic illustration of the activation of a rotaxane crosslinked polymer **10**. (b) Photographs of polymers during tensile tests. (c) Activation of rotaxane crosslinked polymer at 570% elongation. Red arrows indicate the direction of force. Source: Lu et al. [68] / Royal Society Of Chemistry.

(TMI) with DABBF or DABBF-linked [3]rotaxane cross-linkers respectively. Both CP were subjected to tensile tests, and the mechanochromic behavior of DABBF was monitored visually while the formation of the ABF radical was quantified by electron paramagnetic resonance (EPR). Both CCP and RCP form white films when no strain is applied. At maximum strain (CCP: 490%, RCP: 570%), CCP color turns to a deep blue over the entire sample, unlike RCP, which only displays a faint blue domain in the neck of the sample (Figure 1.15b). This picture was confirmed by EPR, where the dissociation rate of RCP was found to be about four times lower than that of CCP. The low degree of activation in the rotaxane cross-linked system was attributed to the slide-ring transition itself (i.e. the mechanical energy is dissipated before the DABBF can be activated) and to a faster recombination of ABF radical in RCP than CCP due to the higher mobility of the rotaxane junction. However, a dissociation of the rotaxane by dethreading cannot be excluded as the 2,5-dimethylphenyl stopper can be easily crossed by the macrocycle under tension [69].

Stoddart' s earliest example of the mechanochemistry of rotaxane-centered polymers involved a change of optical properties due to exposure of a DNP unit after

disruption of CT interaction (Figure 1.10) [57]. However, in this work, the change in optical properties was used only to determine the mechanical change depending on whether the polymer is still intact. More recently, groups have been able to develop mechanical bonds containing mechanochromic devices to give an optical response to a force. Mechanochromic mechanophores have been previously reported [70], but they usually rely on the rupture of a covalent bond and hence require high activation force (nN regime). The ability to sense lower force is particularly desirable to detect mechanobiological processes, which typically occur in the low pN regime [71]. This force regime is the realm of non-covalent interactions, and a rotaxane is an ideal platform to build such a sensor as its subcomponents are often held in place with non-covalent interactions. This strategy was recently used by Sagara and Weder to design a mechanochromic rotaxane in which a fluorophore-bearing macrocycle is wrapped around an electron-poor aromatic quencher [72]. The rotaxane consists of a 1,5-dinaptho[38]crown-10 macrocycle modified with a 4,7-bis(phenylethynyl)-2,1,3-benzothiadiazole (BTH) fluorophore around an axle containing a 1,4,5,8-napthalenetetracarbocyclic diimide (NpI) quencher. As tension is applied, the macrocycle moves away from the quencher and green emission is observed; the emission then immediately disappears as the film is stretched and released, and the macrocycle can re-locate to the quencher (Figure 1.16a,b).

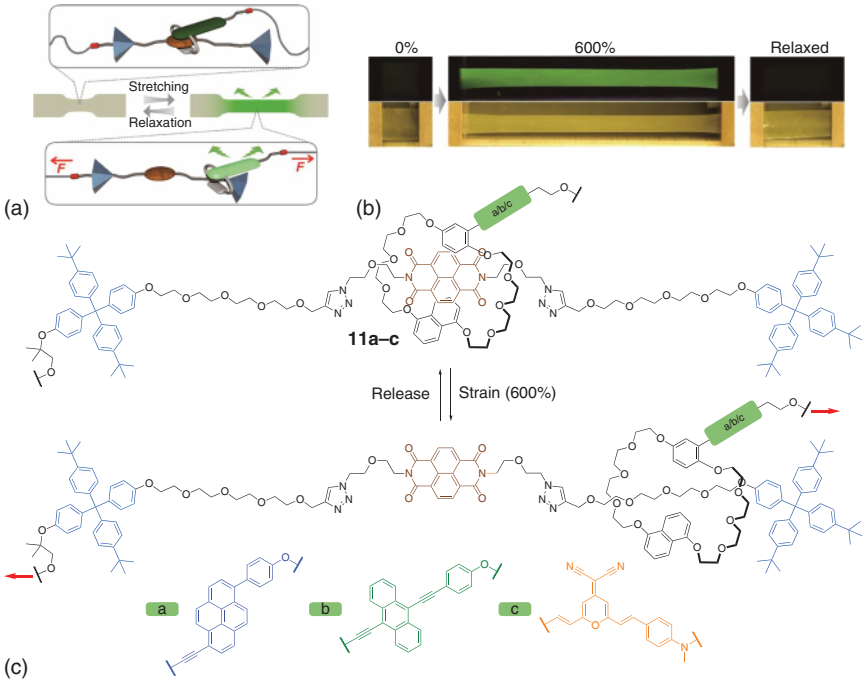


**Figure 1.16** (a) Schematic illustration of reversible rotaxane mechanophores **11a–c**. (b) Photographs of mechanophore-containing thin film during elongation. (c) Activation of rotaxane mechanophores at 600% elongation. Red arrows indicate the direction of force. Source: Sagara et al. [72] / American Chemical Society.

Changing the luminophore part gives access to blue (π-extended pyrene), green (π-extended anthracene), and orange (π-extended 4-(dicyanomethylene)-2methyl-6-(4-dimethylaminostyryl)-4*H*-pyran) photoluminescence (Figure 1.16c). A white-light emission elastomer can be built by combining **11a–c** rotaxanes in the same elastomer [73].

These systems can be activated at low force in a reversible fashion, as they only require the rupture of non-covalent interactions between the macrocycle and its station. However, this design does not enable the fine-tuning of the activation force as the optical and mechanical responses are coupled. In addition, some applications would benefit from an irreversible activation. For example, when the stress history of the material is important (e.g. to indicate when a material has experienced a certain deformation). To address this challenge, Sagara, Weder, and coworkers reported a rotaxane-based mechanophore that can display both reversible and irreversible responses depending on the magnitude of the applied force (Figure 1.17a) [74]. At low tension, the macrocycle is pulled away from the quencher, but it is still retained

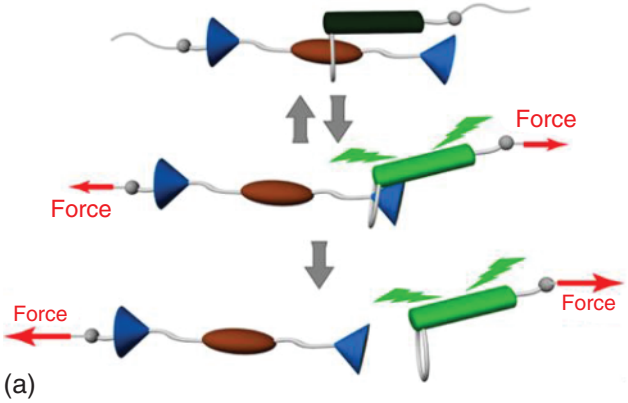


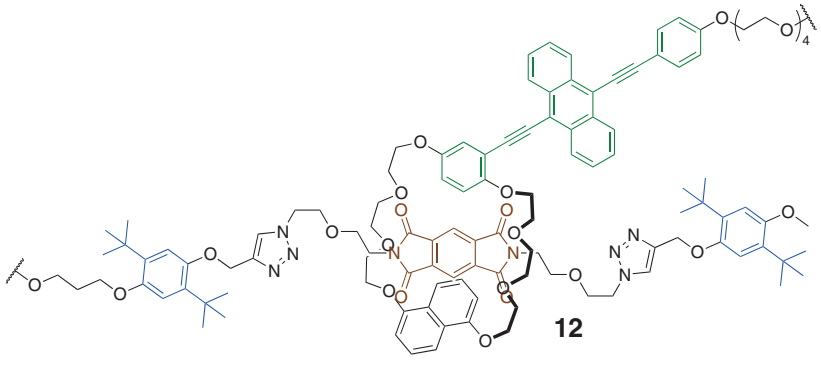


**Figure 1.17** (a) Schematic illustration of reversible and irreversible rotaxane mechanophores; red arrows indicate the direction of force. (b) Example structure of dual response rotaxane mechanophore **12**. Source: Muramatsu et al. [74] / American Chemical Society.

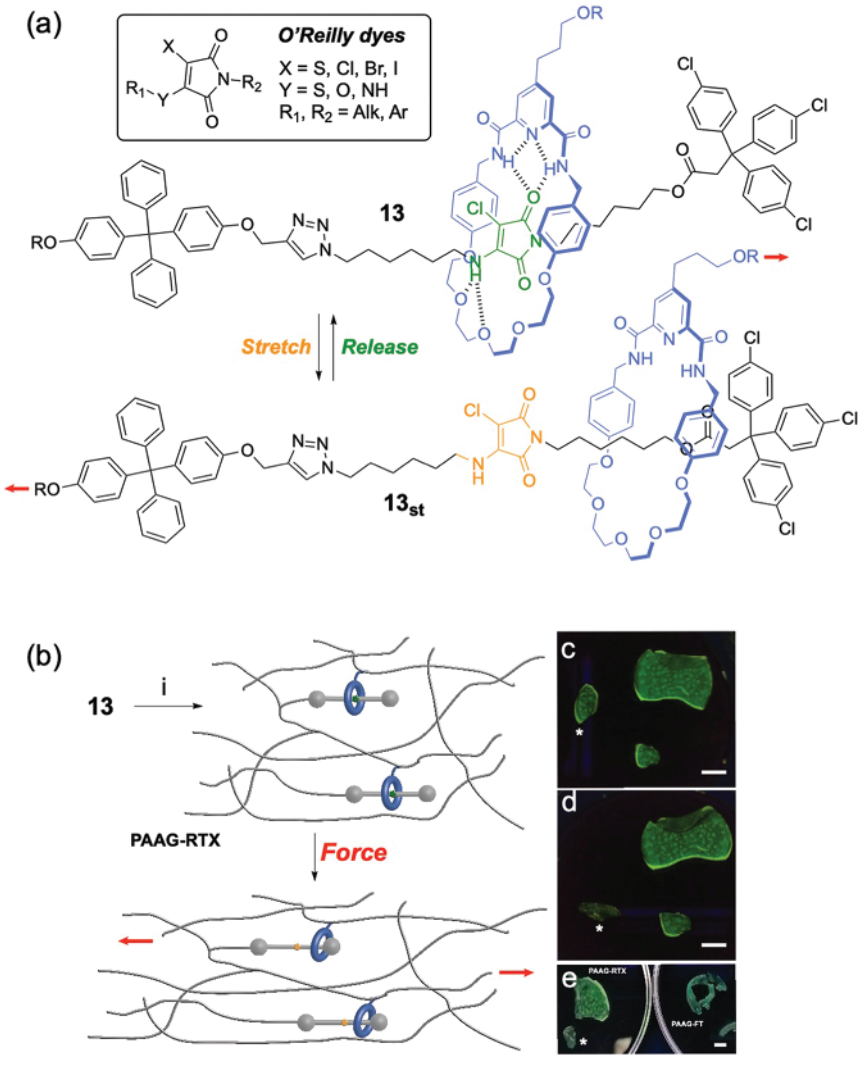


**Figure 1.18** (a) Activation of a mechanochromic hydrogen-bonded rotaxane **13** containing ACM O'Reilly dye after compression. (b) Schematic illustration of force applied to polyacrylamide gel containing rotaxane mechanophore as cross-linker, red arrows indicates the direction of force. Conditions (i) acrylamide (12% w/v), bis-acrylamide (0.3% w/v), rotaxane 1 (0.3% w/v), *N*,*N*,*N*′,*N*′-tetramethylethylenediamine, $(NH_4)_2S_2O_8$, $THF/H_2O$ (1 : 1). (c) Fragments of rotaxane crosslinked gel under 254 nm UV light. (d) The same fragments after compression of * with tweezers for 5 s. (e) comparison of compressed * and native PAAG-RTX fragments with PAAG-FT. Scale bar = 5 mm. Source: Sandoval-Torrientes et al. [75] / John Wiley & Sons / CC BY 4.0.

by the stopper, and releasing the tension restores the initial state. Beyond a certain force threshold, the macrocycle can be pulled over the stopper, and the activation is irreversible. This feat is achieved with a smaller stopper (*p*-di-*tert*-butylphenyl) than in the previous design (Figure 1.17b). Consequently, the size of the macrocycle has been reduced, and a smaller pyromellitic diimide quenching unit is used. Reversible activation of thin film of polyurethane elastomers incorporating the rotaxane (0.05 mol%) was achieved over 50 strain/release cycles (300% maximal strain). However, when the strain was increased to 600%, the emission intensity in the relaxed state increased gradually with the number of cycles and the applied strain. The effect was more prominent at higher strain, which suggests an increasing amount of irreversible activation by dethreading. This study shows how a small change in the architecture of a rotaxane can result in both reversible and irreversible responses to force. Notably, the rotaxanes that become dethreaded over time can allow for the recording of the mechanical history of a material undergoing repeated stain as an optical signal.

In 2021, De Bo and coworkers were able to introduce a rotaxane force sensor into a polyacrylamide gel (PAAG), which can serve as a model for living tissue [75]. The rotaxane **13** is centered around an aminochloromaleimide (ACM) derivative (O'Reilly dye) [76], which acts as both a fluorescent dye and a recognition motif for the macrocycle (Figure 1.18a). These dyes exhibit a strong emission due to their donor–acceptor architecture, which is quenched in the presence of a strong hydrogen bond donor [77]. Additionally, their optical properties can be tuned by altering the substitution pattern [78]. It was hypothesized that the macrocycle, containing both a hydrogen bond donor unit (pyridyl-2,6-dicarboxyamide) and a hydrogen bond acceptor crown ether-like region, would be a suitable host for the ACM unit and that the fluorescence of ACM would be altered due to the presence of two electron-rich aromatic flanking groups and the hydrogen bond network (Figure 1.18a). The rotaxane was incorporated as a cross-linker in a PAAG, a popular matrix model to mimic living tissues due to their similar viscoelastic properties (Figure 1.18b). The green fluorescence of the resulting PAAG-RTX gel is greatly reduced when the gel is compressed (Figure 1.18c–e); however, the activation proved irreversible, probably due to stronger hydrogen bonds between polar groups in the gel and components of the rotaxane, than between the components themselves (i.e. between the dye and the macrocycle). Though a reversible activation was not achieved, this system offers a versatile platform for the assembly of a force sensor for *in vivo* applications.

## 1.5 Conclusions

As the number and complexity of mechanical bonds expand, new force-responsive transformations will become available. SMFS and ultrasound activation can work hand-in-hand to uncover new and interesting dissociation pathways and the real-time events leading to bond cleavage. The different ways in which rotaxanes and catenanes direct force will have important applications in the design of future materials containing these architectures, which will be subjected to high force,

either accelerating the cleavage or shielding specific sites from force. The way that component parts can be pulled either toward or away from each other can be exploited to unlock new reactivity within the mechanical bond structure. Continuous development of force-responsive materials could result in increased responses to multiple levels of force, allowing for materials to display more detailed information on the stress applied and offering a wider range of potential applications in different settings.

## References


1 Bruns, C.J. and Stoddart, J.F. (2016). *The Nature of the Mechanical Bond*. Hoboken, NJ: Wiley.
2 De Bo, G. (2018). Mechanochemistry of the mechanical bond. *Chem. Sci.* 9 (1): 15–21.
3 Hinterdorfer, P. and Dufrêne, Y.F. (2006). Detection and localization of single molecular recognition events using atomic force microscopy. *Nat. Methods* 3 (5): 347–355.
4 Neuman, K.C. and Nagy, A. (2008). Single-molecule force spectroscopy: optical tweezers, magnetic tweezers and atomic force microscopy. *Nat. Methods* 5 (6): 491–505.
5 Mora, M., Stannard, A., and Garcia-Manyes, S. (2020). The nanomechanics of individual proteins. *Chem. Soc. Rev.* 49 (19): 6816–6832.
6 Bustamante, C., Chemla, Y.R., Forde, N.R., and Izhaky, D. (2004). Mechanical Processes in Biochemistry. *Annu. Rev. Biochem.* 73 (1): 705–748.
7 Bustamante, C. et al. (2008). Single-molecule theme. *Annu. Rev. Biochem.* 77 (1): 45–228.
8 Müller, D.J. and Dufrêne, Y.F. (2008). Atomic force microscopy as a multifunctional molecular toolbox in nanobiotechnology. *Nat. Nanotechnol.* 3 (5): 261–269.
9 Puchner, E.M. and Gaub, H.E. (2009). Force and function: probing proteins with AFM-based force spectroscopy. *Curr. Opin. Struct. Biol.* 19 (5): 605–614.
10 Liang, J. and Fernández, J.M. (2009). Mechanochemistry: one bond at a time. *ACS Nano* 3 (7): 1628–1645.
11 Duwez, A.-S. and Willet, N. (ed.) (2011). *Molecular Manipulation with Atomic Force Microscopy*. CRC Press.
12 Marszalek, P.E. and Dufrêne, Y.F. (2012). Stretching single polysaccharides and proteins using atomic force microscopy. *Chem. Soc. Rev.* 41 (9): 3523.
13 Žoldák, G. and Rief, M. (2013). Force as a single molecule probe of multidimensional protein energy landscapes. *Curr. Opin. Struct. Biol.* 23 (1): 48–57.
14 Hughes, M.L. and Dougan, L. (2016). The physics of pulling polyproteins: a review of single molecule force spectroscopy using the AFM to study protein unfolding. *Rep. Prog. Phys.* 79 (7): 076601.
15 Nathwani, B., Shih, W.M., and Wong, W.P. (2018). Force spectroscopy and beyond: innovations and opportunities. *Biophys. J.* 115 (12): 2279–2285.

**16** Bao, Y., Luo, Z., and Cui, S. (2020). Environment-dependent single-chain mechanics of synthetic polymers and biomacromolecules by atomic force microscopy-based single-molecule force spectroscopy and the implications for advanced polymer materials. *Chem. Soc. Rev.* 49 (9): 2799–2827.

**17** Brown, C.L. and Craig, S.L. (2015). Molecular engineering of mechanophore activity for stress-responsive polymeric materials. *Chem. Sci.* 6 (4): 2158–2165.

**18** Ghanem, M.A., Basu, A., Behrou, R. et al. (2021). The role of polymer mechanochemistry in responsive materials and additive manufacturing. *Nat. Rev. Mater.* 6 (1): 84–98.

**19** Bowser, B.H., Wang, S., Kouznetsova, T.B. et al. (2021). Single-event spectroscopy and unravelling kinetics of covalent domains based on cyclobutane mechanophores. *J. Am. Chem. Soc.* 143 (13): 5269–5276.

**20** Zhang, Y., Wang, Z., Kouznetsova, T.B. et al. (2021). Distal conformational locks on ferrocene mechanophores guide reaction pathways for increased mechanochemical reactivity. *Nat. Chem.* 13 (1): 56–62.

**21** Janke, M., Rudzevich, Y., Molokanova, O. et al. (2009). Mechanically interlocked calix[4]arene dimers display reversible bond breakage under force. *Nat. Nanotechnol.* 4 (4): 225–229.

**22** Xing, H., Li, Z., Wang, W. et al. (2020). Mechanochemistry of an interlocked poly[2]catenane: from single molecule to bulk gel. *CCS Chem.* 2 (1): 513–523.

**23** Sluysmans, D., Zhang, L., Li, X. et al. (2020). Viologen tweezers to probe the force of individual donor–acceptor π-interactions. *J. Am. Chem. Soc.* 142 (50): 21153–21159.

**24** Devaux, F., Li, X., Sluysmans, D. et al. (2021). Single-molecule mechanics of synthetic aromatic amide helices: ultrafast and robust non-dissipative winding. *Chem* 7 (5): 1333–1346.

**25** Lussis, P., Svaldo-Lanero, T., Bertocco, A. et al. (2011). A single synthetic small molecule that generates force against a load. *Nat. Nanotechnol.* 6 (9): 553–557.

**26** Van Quaethem, A., Lussis, P., Leigh, D.A. et al. (2014). Probing the mobility of catenane rings in single molecules. *Chem. Sci.* 5 (4): 1449.

**27** Naranjo, T., Lemishko, K.M., de Lorenzo, S. et al. (2018). Dynamics of individual molecular shuttles under mechanical force. *Nat. Commun.* 9 (1): 4512.

**28** Sluysmans, D., Hubert, S., Bruns, C.J. et al. (2018). Synthetic oligorotaxanes exert high forces when folding under mechanical load. *Nat. Nanotechnol.* 13 (3): 209–213.

**29** Sluysmans, D., Devaux, F., Bruns, C.J. et al. (2018). Dynamic force spectroscopy of synthetic oligorotaxane foldamers. *Proc. Natl. Acad. Sci.* 115 (38): 9362–9366.

**30** Sluysmans, D., Lussis, P., Fustin, C.-A. et al. (2021). Real-time fluctuations in single-molecule rotaxane experiments reveal an intermediate weak binding state during shuttling. *J. Am. Chem. Soc.* 143 (5): 2348–2352.

**31** Brough, B., Northrop, B.H., Schmidt, J.J. et al. (2006). Evaluation of synthetic linear motor-molecule actuation energetics. *Proc. Natl. Acad. Sci.* 103 (23): 8583–8588.

**32** Altieri, A., Bottari, G., Dehez, F. et al. (2003). Remarkable positional discrimination in bistable light- and heat-switchable hydrogen-bonded molecular shuttles. *Angew. Chem. Int. Ed.* 42 (20): 2296–2300.

**33** Ashton, P.R., Baxter, I., Fyfe, M.C.T. et al. (1998). Rotaxane or pseudorotaxane? That is the question! *J. Am. Chem. Soc.* 120 (10): 2297–2307.

**34** Affeld, A., Hübner, G.M., Seel, C., and Schalley, C.A. (2001). Rotaxane or pseudorotaxane? Effects of small structural variations on the deslipping kinetics of rotaxanes with stopper groups of intermediate size. *Eur. J. Org. Chem.* 2001 (15): 2877.

**35** McGonigal, P.R., Li, H., Cheng, C. et al. (2015). Controlling association kinetics in the formation of donor–acceptor pseudorotaxanes. *Tetrahedron Lett.* 56 (23): 3591–3594.

**36** Gómez-Durán, C.F.A., Liu, W., de Lourdes Betancourt-Mendiola, M., and Smith, B.D. (2017). Structural control of kinetics for macrocycle threading by fluorescent squaraine dye in water. *J. Org. Chem.* 82 (16): 8334–8341.

**37** Martinez-Cuezva, A., Rodrigues, L.V., Navarro, C. et al. (2015). Dethreading of tetraalkylsuccinamide-based [2]rotaxanes for preparing benzylic amide macrocycles. *J. Org. Chem.* 80 (20): 10049–10059.

**38** Saito, S., Takahashi, E., Wakatsuki, K. et al. (2013). Synthesis of large [2]rotaxanes. The relationship between the size of the blocking group and the stability of the rotaxane. *J. Org. Chem.* 78 (8): 3553–3560.

**39** Clifford, T., Abushamleh, A., and Busch, D.H. (2002). Factors affecting the threading of axle molecules through macrocycles: binding constants for semirotaxane formation. *Proc. Natl. Acad. Sci.* 99 (8): 4830–4836.

**40** Heim, C., Affeld, A., Nieger, M., and Vögtle, F. (1999). Size complementarity of macrocyclic cavities and stoppers in amide-rotaxanes. *Helv. Chim. Acta* 82 (5): 746–759.

**41** Raymo, F.M., Houk, K.N., and Stoddart, J.F. (1998). The mechanism of the slippage approach to rotaxanes. Origin of the "all-or-nothing" substituent effect. *J. Am. Chem. Soc.* 120 (36): 9318–9322.

**42** Wenz, G., Han, B.-H., and Müller, A. (2006). Cyclodextrin rotaxanes and polyrotaxanes. *Chem. Rev.* 106 (3): 782–817.

**43** Dunlop, A., Wattoom, J., Hasan, E.A. et al. (2008). Mapping the positions of beads on a string: dethreading rotaxanes by molecular force spectroscopy. *Nanotechnology* 19 (34): 345706.

**44** Bowman, K.A., Aarstad, O.A., Stokke, B.T. et al. (2016). Sliding contact dynamic force spectroscopy method for interrogating slowly forming polymer cross-links. *Langmuir* 32 (48): 12814–12822.

**45** Dunlop, A., Bowman, K., Aarstad, O. et al. (2017). Polymer sequencing by molecular machines: a framework for predicting the resolving power of a sliding contact force spectroscopy sequencing method. *Nanoscale* 9 (39): 15089–15097.

**46** Evans, E. and Ritchie, K. (1997). Dynamic strength of molecular adhesion bonds. *Biophys. J.* 72 (4): 1541–1555.

**47** Friddle, R.W., Noy, A., and De Yoreo, J.J. (2012). Interpreting the widespread nonlinear force spectra of intermolecular bonds. *Proc. Natl. Acad. Sci.* 109 (34): 13573–13578.

**48** Li, J., Nagamani, C., and Moore, J.S. (2015). Polymer mechanochemistry: from destructive to productive. *Acc. Chem. Res.* 48 (8): 2181–2190.

**49** Klein, I.M., Husic, C.C., Kovács, D.P. et al. (2020). Validation of the CoGEF method as a predictive tool for polymer mechanochemistry. *J. Am. Chem. Soc.* 142 (38): 16364–16381.

**50** Nixon, R. and De Bo, G. (2020). Three concomitant C–C dissociation pathways during the mechanical activation of an *N*-heterocyclic carbene precursor. *Nat. Chem.* 12 (9): 826–831.

**51** Liu, Y., Holm, S., Meisner, J. et al. (2021). Flyby reaction trajectories: chemical dynamics under extrinsic force. *Science* 373 (6551): 208–212.

**52** Lenhardt, J.M., Ong, M.T., Choe, R. et al. (2010). Trapping a diradical transition state by mechanochemical polymer extension. *Science* 329 (5995): 1057–1060.

**53** Chen, Z., Mercer, J.A.M., Zhu, X. et al. (2017). Mechanochemical unzipping of insulating polyladderene to semiconducting polyacetylene. *Science* 357 (6350): 475–479.

**54** Piermattei, A., Karthikeyan, S., and Sijbesma, R.P. (2009). Activating catalysts with mechanical force. *Nat. Chem.* 1 (2): 133–137.

**55** Michael, P. and Binder, W.H. (2015). A mechanochemically triggered "click" catalyst. *Angew. Chem. Int. Ed.* 54 (47): 13918–13922.

**56** Küng, R., Göstl, R., and Schmidt, B.M. (2022). Release of molecular cargo from polymer systems by mechanochemistry. *Chem. Eur. J.* 28 (17): e202103860.

**57** Stoll, R.S., Friedman, D.C., and Stoddart, J.F. (2011). Mechanically interlocked mechanophores by living-radical polymerization from rotaxane initiators. *Org. Lett.* 13 (10): 2706–2709.

**58** May, P.A. and Moore, J.S. (2013). Polymer mechanochemistry: techniques to generate molecular force via elongational flows. *Chem. Soc. Rev.* 42 (18): 7497.

**59** De Bo, G. (2022). Mechanochemical dethreading of a cyclobis(paraquat-*p*-phenylene)-derived [2]rotaxane. figshare. Figure. https://doi.org/10.6084/m9.figshare.20153708.v1.

**60** Zhang, M. and De Bo, G. (2018). Impact of a mechanical bond on the activation of a mechanophore. *J. Am. Chem. Soc.* 140 (40): 12724–12727.

**61** Stevenson, R. and De Bo, G. (2017). Controlling reactivity by geometry in retro-Diels–Alder reactions under tension. *J. Am. Chem. Soc.* 139 (46): 16768–16771.

**62** Zhang, M. and De Bo, G. (2019). Mechanical susceptibility of a rotaxane. *J. Am. Chem. Soc.* 141 (40): 15879–15883.

**63** Mayumi, K., Ito, K., and Kato, K. (2015). *Polyrotaxane and Slide-Ring Materials*. Cambridge: Royal Society of Chemistry.

**64** Lee, B., Niu, Z., and Craig, S.L. (2016). The mechanical strength of a mechanical bond: sonochemical polymer mechanochemistry of poly(catenane) copolymers. *Angew. Chem. Int. Ed.* 55 (42): 13086–13089.

**65** Zhang, M. and De Bo, G. (2020). A catenane as a mechanical protecting group. *J. Am. Chem. Soc.* 142 (11): 5029–5033.

**66** Davis, D.A., Hamilton, A., Yang, J. et al. (2009). Force-induced activation of covalent bonds in mechanoresponsive polymeric materials. *Nature* 459 (7243): 68–72.

**67** Imato, K., Irie, A., Kosuge, T. et al. (2015). Mechanophores with a reversible radical system and freezing-induced mechanochemistry in polymer solutions and gels. *Angew. Chem. Int. Ed.* 54 (21): 6168–6172.

**68** Lu, Y., Aoki, D., Sawada, J. et al. (2020). Visualization of the slide-ring effect: a study on movable cross-linking points using mechanochromism. *Chem. Commun.* 56 (23): 3361–3364.

**69** De Bo, G. (2022). Mechanochemical dethreading of a dibenzo-24-crown-8 (DB24C8) macrocycle connected to a diaryl-bibenzofuranone (DABBF) mechanochromophore. figshare. Figure. https://doi.org/10.6084/m9.figshare.20340873.v1.

**70** Chen, Y., Mellot, G., van Luijk, D. et al. (2021). Mechanochemical tools for polymer materials. *Chem. Soc. Rev.* 50 (6): 4100–4140.

**71** Roca-Cusachs, P., Conte, V., and Trepat, X. (2017). Quantifying forces in cell biology. *Nat. Cell Biol.* 19 (7): 742–751.

**72** Sagara, Y., Karman, M., Verde-Sesto, E. et al. (2018). Rotaxanes as mechanochromic fluorescent force transducers in polymers. *J. Am. Chem. Soc.* 140 (5): 1584–1587.

**73** Sagara, Y., Karman, M., Seki, A. et al. (2019). Rotaxane-based mechanophores enable polymers with mechanically switchable white photoluminescence. *ACS Cent. Sci.* 5 (5): 874–881.

**74** Muramatsu, T., Okado, Y., Traeger, H. et al. (2021). Rotaxane-based dual function mechanophores exhibiting reversible and irreversible responses. *J. Am. Chem. Soc.* 143 (26): 9884–9892.

**75** Sandoval-Torrientes, R., Carr, T., and De Bo, G. (2021). A mechanochromic hydrogen-bonded rotaxane. *Macromol. Rapid Commun.* 42 (1): 2000447.

**76** Robin, M.P., Wilson, P., Mabire, A.B. et al. (2013). Conjugation-induced fluorescent labeling of proteins and polymers using dithiomaleimides. *J. Am. Chem. Soc.* 135 (8): 2875–2878.

**77** Mabire, A.B., Robin, M.P., Quan, W.-D. et al. (2015). Aminomaleimide fluorophores: a simple functional group with bright, solvent dependent emission. *Chem. Commun.* 51 (47): 9733–9736.

**78** Xie, Y., Husband, J.T., Torrent-Sucarrat, M. et al. (2018). Rational design of substituted maleimide dyes with tunable fluorescence and solvafluorochromism. *Chem. Commun.* 54 (27): 3339–3342.